MATERIALS CHEMISTRY FRONTIERS

RESEARCH ARTICLE

View Article Online
View Journal | View Issue

Cite this: *Mater. Chem. Front.*, 2024, **8**, 2764

High performance inverted planar perovskite solar cells enhanced by heteroatomic functionalized hole transport materials†

Zheng Xie,[ac] Yuheng Li,[c] Xuehui Li,[a] Yizhen Fang,[b] Jinrui Chang,[b] Qiong Yang,[a] Xiaowen Sun,[a] Chunyang Miao,[a] Gang Lu,[a] Zhangxin Chen,[b] Gongqiang Li,*[b] Yanxian Jin,*[b] Zhoulu Wang*[d] and Xiong Li*[c]

Two organic small molecule hole transport materials, 5-((3,6-bis(4-(bis(4-methoxyphenyl)amino)phenyl)-thieno[3,2-*b*]thiophen-2-yl)methylene)-3-ethyl-2-thioxothiazolidin-4-one (shortly named C3-D) and 5,5′-((3,6-bis(4-(bis(4-methoxyphenyl)amino)phenyl)thieno[3,2-*b*]thiophene-2,5-diyl)bis(methaneylylidene))bis(3-ethyl-2-thioxothiazolidin-4-one) (shortly named C3-S), are designed with rhodanine as the functional group and utilized in inverted planar perovskite solar cells (PSCs). With the functional group, both HTMs exhibit good mobility, matching HOMO/LUMO energy levels and excellent interactions with ITO and the perovskite layer, enhancing hole extraction, transport, and defect passivation in inverted PSCs. As a result, the device based-on C3-D presents a champion power conversion efficiency (PCE) of 21.50% with J_{SC} = 24.49 mA cm^{-2}, V_{OC} = 1.072 V, and FF = 81.9%, while the device based-on C3-S shows a PCE of 19.24% with J_{SC} = 23.11 mA cm^{-2}, V_{OC} = 1.065 V, and FF = 78.2%. Additionally, the C3-D-based device also demonstrates superior stability compared to C3-S, retaining over 85% of the initial value after being kept for 500 h at room temperature in ambient air at 35% relative humidity, and over 60% of the initial value after being kept for 500 h at 85 °C in a N_2 glovebox, respectively. These results far surpass the performance of devices based-on a non-functional HTM, TT-3,6-TPA, as reported in the literature (a PCE of 0.7% with J_{SC} = 2.90 mA cm^{-2}, V_{OC} = 0.95 V, and FF = 27.0%). Therefore, these findings indicate that combining hetero-atomic functionalized groups with typical hole transport fragments could be a promising research avenue for enhancing the performance of inverted planar PSCs and facilitating the commercialization of perovskite solar cells.

Received 21st May 2024,
Accepted 14th June 2024

DOI: 10.1039/d4qm00417e

rsc.li/frontiers-materials

1. Introduction

With the growing environmental and energy challenges, renewable energy has become the focus of research. Among the studies, photovoltaic technology has become a key area of research. Over the last decade, perovskite has been identified as an ideal photovoltaic material[1–3] due to its low manufacturing costs, exceptional charge-carrier mobility, long diffusion range, and broad absorption,[4] prompting extensive research.[5] As a result, perovskite solar cells (PSCs) have experienced rapid development, with the power conversion efficiency (PCE) rising from the initial 3.8%[6] to the latest 26.1%,[7] approaching the efficiency of state-of-the-art crystalline-silicon solar cells. An inverted planar PSC is an excellent type of photovoltaic solar cell with promising applications,[8] particularly in tandem solar cells,[9] large-area PSCs,[10] and flexible PSCs.[11] To improve the efficiency and stability of inverted planar PSCs,[12] hole transport materials (HTMs) play crucial roles as an intermediate layer between the electrode and perovskite layer. They are crucial for inverted planar PSCs not only in hole extracting and transporting, and electron blocking,[13] but also in influencing the nucleation, crystallization, and optimization of the morphology of the perovskite film.[14] Additionally, they also can enhance the interactions between the electrode and the perovskite layer,[15] benefitting the improvement of the efficiency and stability of PSCs by passivating buried surface defects of perovskite,[16] and partially

[a] *Institute of Advanced Materials (IAM), Nanjing Tech University (NanjingTech), 30 South Puzhu Road, Nanjing 211816, P. R. China*
[b] *School of Pharmaceutical and Chemical Engineering, Taizhou University, Jiaojiang, Zhejiang 318000, P. R. China. E-mail: Ligq6081@163.com, shirleyj@tzc.edu.cn*
[c] *Wuhan National Laboratory for Optoelectronics (WNLO), Huazhong University of Science and Technology (HUST), Luoyu Road 1037, Wuhan 430074, Hubei, P. R. China. E-mail: xiongli@sustech.edu.cn*
[d] *School of Energy Science and Engineering, Nanjing Tech University (NanjingTech), 30 South Puzhu Road, Nanjing 211816, P. R. China. E-mail: zlwang@njtech.edu.cn*

† Electronic supplementary information (ESI) available: The experimental details, characterization of HTMs, and thermogravimetric analysis and other related results, supplied as ESI. See DOI: https://doi.org/10.1039/d4qm00417e

blocking moisture and oxygen to a certain extent.[17] So, it is crucial to develop high-efficient HTMs for high-performance perovskite solar cells.

Generally, over the last few decades, numerous HTMs have been developed, including both inorganic and organic varieties. Inorganic HTMs, despite their many advantages such as high hole mobility, matched energy levels, excellent stability, and low cost, still face several critical challenges as outlined below:[18] (a) it is difficult to form high-quality compact films with inorganic HTMs because of agglomeration caused by their nano-particles; (b) negative effects on hole extraction and transportation[19] are caused by the roughness and high-density of defects in the inorganic HTM layer; and (c) additional interface layers are usually necessary[20–22] because the direct contact between inorganic HTMs and perovskite layers tends to accelerate the degradation of perovskite, leading to decreased efficiency and stability of PSCs. For example, Sungjin Park *et al.* introduced a relatively neutral ammonium salt into NiO_x solution, resulting in the achievement of a champion PCE of 19.91% based on $MAPbI_3$.[18]

Compared to inorganic HTMs, the organic ones offer several advantages, including good solubility, diverse structures, and tunable energy levels, leading to good compatibility with various perovskite compositions. Additionally, organic HTMs usually contain a wide range of functional groups with various heteroatoms and form dense and smooth films easily. These can enhance the interactions with electrodes or perovskite layers, and facilitate the nucleation, crystallization, and surface defect passivation of perovskite layers, benefiting the PSC performance by reducing the interface non-radiative recombination and leak currents.[23]

In organic HTMs, polymers such as PTAA,[24] PEDOT:PSS[25] and P3HT[26] are commonly used in inverted PSCs and exhibit excellent PCEs. However, the stability and repeatability of these PSC devices are poor due to the uncertainty of these polymer molecular weight and poor batch-to-batch reproducibility. Additionally, organic polymer materials have the potential for dispersion and agglomeration issues in solution to some extent and are also too expensive to be used in large-scale fabrication of PSCs. Therefore, organic small molecule hole transport materials have been increasingly studied because of their well-defined structure, simple synthesis, and good batch-to-batch reproducibility.[27]

To improve the efficiency and stability of perovskite solar cells, scientists have recently focused on using small molecule passivation to address surface defects on perovskite crystals with heteroatom functional groups.[28] This helps to reduce non-radiative recombination in grain boundaries and interfaces between the hole/electron and the perovskite layer, enhance the interaction and interface dipole interaction between the perovskite and the charge transport layer,[29–32] and improve the efficiency of charge separation and transport.[15,33–35] Especially, *via* the implementation of self-assembled molecules (SAMs) in inverted PSCs, numerous functionalized HTMs have been created,[36–39] and currently, the PCE based on functionalized HTMs exceeds 22%.[40–42]

Inspired by these concepts, we have created two new organic small molecule HTMs, 5-((3,6-bis(4-(bis(4-methoxyphenyl)amino)-phenyl)thieno[3,2-*b*]thiophen-2-yl)methylene)-3-ethyl-2-thioxothiazolidin-4-one (shortly named C3-D) and 5,5′-((3,6-bis(4-(bis(4-methoxyphenyl)amino)phenyl)thieno[3,2-*b*]thiophene-2,5-diyl)bis-(methaneylylidene))bis(3-ethyl-2-thioxothiazolidin-4-one) (shortly named C3-S) by functionalizing TT-3,6-TPA[43] with rhodanine groups (Fig. 1). Here, the triphenylamine (TPA) and thienothiophene (TT) units are frequently utilized in high mobility organic semiconductors like OPVs, OLEDs, and OFETs. These units can guarantee that the new HTMs possess high mobility and good thermal, morphological, and optoelectrochemical properties, which are advantageous for hole extraction and transport. Meanwhile, the rhodanine structural unit can enhance the interactions between the HTM and the electrode and the perovskite layer, improve interfacial contact, and reduce surface defects at the bottom interface of the perovskite layer, all of which can improve charge extraction and transport, and suppress non-radiative recombination of charges. As anticipated, the functionalized HTMs, C3-D and C3-S, exhibit robust interactions with the electrode and perovskite layer, respectively, effectively passivating surface defects. Additionally, both HTMs demonstrate a precise alignment of HOMO energy levels with the perovskite layer. These advantages collectively contribute to the enhanced performance of PSCs. As a result, the best PSC device based on C3-D achieves a champion PCE of 21.50% with J_{SC} of 24.49 mA cm^{-2}, V_{OC} of 1.072 V, and FF of 81.9% under the standard AM 1.5G illumination, while the device based-on C3-S demonstrates a PCE of 19.24% with J_{SC} = 23.11 mA cm^{-2}, V_{OC} = 1.065 V, and FF = 78.2% under the same conditions. All these results far surpass the performance of devices based on a non-functional similar HTM, TT-3,6-TPA, as reported in the literature[43] (the highest PCE of 0.7% with J_{SC} = 2.90 mA cm^{-2}, V_{OC} = 0.95 V, and FF = 27.0%). Notably, both devices based on C3-D and C3-S demonstrate very good stabilities, retaining over 90% of the initial value after being stored for 500 hours at 25 °C in a N_2 glovebox, while being heated for over 500 hours at 85 °C in a N_2 glovebox, the device based on C3-D displays better stability with 60% of its initial PCE being retained compared C3-S. Additionally, after being aged for 500 hours in ambient air at 35% relative humidity at room temperature, the power conversion efficiency (PCE) of the device using C3-D retains 85% of its initial value. In contrast, after only 200 hours of aging, the PCE of the device using C3-S decreases to 85% of its initial value. All these results prove that the hetero-atomic functional strategy offers a highly efficient pathway to develop HTMs for high-performance inverted planar PSCs.

2. Results and discussion

2.1. Synthesis and properties of C3-D and C3-S

The HTMs C3-D and C3-S are synthesized (Fig. S1–S4, ESI†), from commercially available compounds 4-methoxy-*N*-(4-methoxyphenyl)-*N*-(4-(4,4,5,5-tetramethyl-1,3,2-dioxaborolan-2-yl)phenyl)aniline and 3,6-dibromothieno[3,2-*b*]thiophene through a simple three-step reaction with good yield.[43–45] Their structures are determined using ^{1}H NMR, ^{13}C NMR, and FT-MS spectra (Fig. S5–S9, ESI†). The thermal properties of these two HTMs are determined through thermogravimetric analysis (TGA) and differential

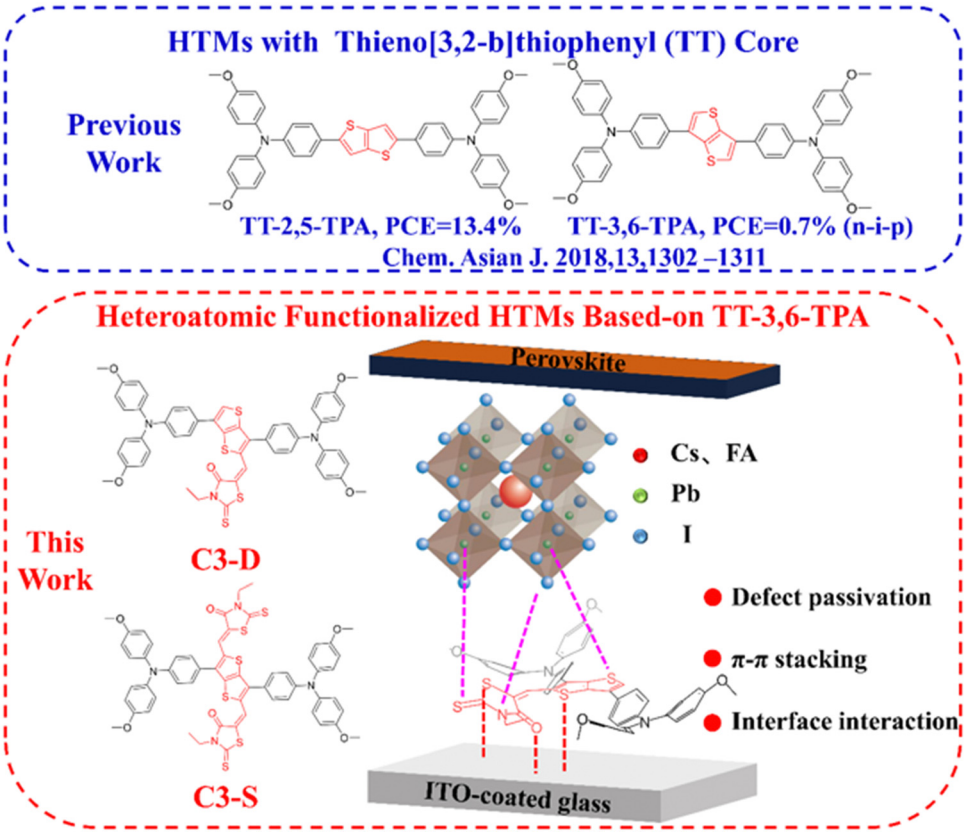

Fig. 1 Organic small molecule HTMs with TT-TPA and our strategy.

scanning calorimetry (DSC) measurements (Fig. S10, ESI†). Both C3-D and C3-S showed outstanding thermal stabilities in TGA tests, with 5% weight loss observed at 401 °C and 396 °C, respectively. These decomposition temperatures also ensure sufficient thermal stability for the annealing process in the fabrication of PSCs. DSC scans reveal that the glass transition temperature (T_g) of C3-D is 135 °C, whereas no distinct T_g is detected for C3-S, with both being inherently in amorphous phases. The outstanding thermal stability would benefit the stability of PSCs. To investigate their optical properties, the ultraviolet-visible (UV-vis) absorption spectra of C3-D and C3-S in dilute CH_2Cl_2 solution and thin films (quartz substrate) are measured. As depicted in Fig. 2a, both the film and solution of C3-D exhibit a $\lambda_{abs/max}$ value of around 434 nm with another obvious absorption peak at ~520 nm, while those of C3-S show a $\lambda_{abs/max}$ value of around 519 nm with a very slight shoulder peak at ~600 nm. The difference in $\lambda_{abs/max}$ between C3-D and C3-S can be attributed to the intramolecular charge transfer throughout the molecule and the effect of the electron-withdrawing groups, rhodanine. Both the absorption spectra of C3-D and C3-S films show only a slight redshift compared to those in the solution. This is attributed to the rhodanine group blocking the intermolecular π–π stacking in films, which may decrease the hole mobility between adjacent molecules in PSCs.[46] The significant absorption below 400 nm of both C3-D and C3-S has a strong effect on shielding the perovskite layer from ultraviolet damage and degradation to some extent, thereby contributing to the enhancement of PSC device stability. However, the strong absorption of C3-S at 520 nm may have a negative impact on the light absorption of the upper perovskite layer, leading to a decrease in the performance of inverted planar PSCs. Based on the UV-Vis absorption spectrum, we calculated the optical bandgap of C3-D and C3-S to be 1.98 eV and 1.75 eV, respectively. Additionally, their HOMO/LUMO energy levels were determined through ultraviolet photoelectron spectroscopy (UPS) measurements. As depicted in Fig. S11 (ESI†), the valence regions (E_{onset}) and secondary electron cutoff edges (E_{cutoff}) were found to be −9.66 eV and 6.27 eV for C3-D, and −9.61 eV and 6.36 eV for C3-S, respectively. Based on the results of UPS and UV-Vis absorption measurements, the HOMO/LUMO energy levels of C3-D and C3-S are calculated to be −5.29 eV/−3.31 eV and −5.25 eV/−3.50 eV, respectively.

To assess the hole mobility of C3-D and C3-S, the current density–voltage characteristics of a hole-only device using the ITO/PEDOT:PSS/C3-D and C3-S/MoO_3/Ag structure were obtained and analyzed using the space-charge-limited current (SCLC) model, as depicted in Fig. S12 (ESI†). The hole mobility was found to be 1.29×10^{-4} cm^2 V^{-1} s^{-1} for C3-D and 8.61×10^{-5} cm^2 V^{-1} s^{-1} for C3-S. The higher mobility of C3-D facilitates better charge transport compared to C3-S in PSCs. All the properties of C3-D and C3-S are summarized in Table 1.

2.2. Morphology and interactions between HTMs and ITO

As mentioned earlier, the morphology of a HTM and its interaction with the electrode are crucial for improving the

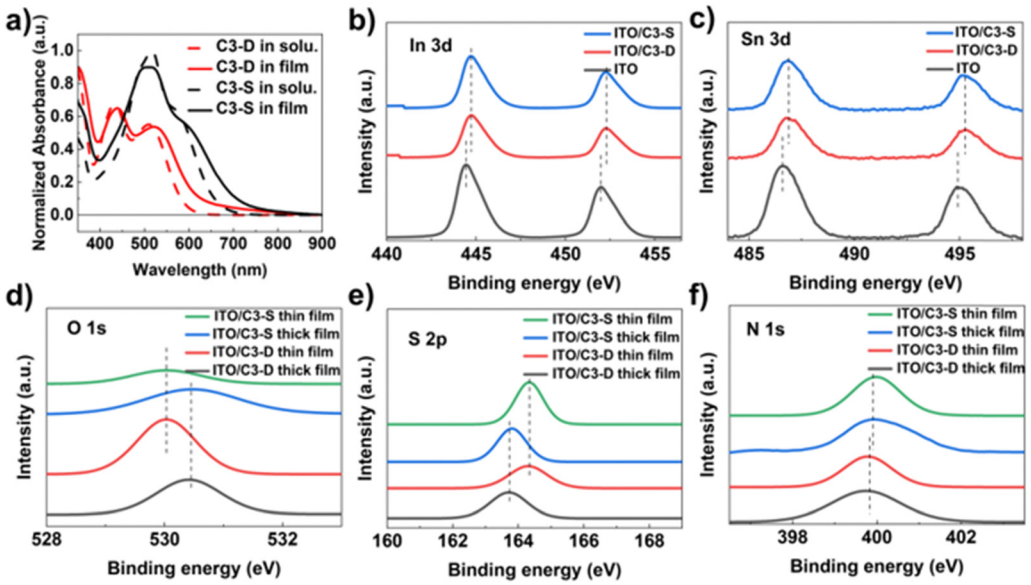

Fig. 2 (a) UV-vis absorption spectra of C3-D and C3-S; XPS spectra of (b) in 3d, (c) Sn 3d, (d) O 1s, (e) S2p, and (f) N1s for C3-D, C3-S deposited on ITO and bare ITO.

efficiency and stability of PSCs. To examine the morphology of C3-D and C3-S on ITO, atomic force microscopy (AFM) tests were performed. The specific data and roughness fluctuation curves can be found in Table S1 and Fig. S14, S15 (ESI†). In Fig. 3f, the surface roughness (Sq) is 21.39 nm (C3-D) and 21.61 nm (C3-S), respectively. The low roughness of the films is beneficial for the deposition of perovskite, contributing to the high quality of the perovskite layer. To investigate the interactions between HTMs and ITO, X-ray photoemission spectra (XPS) were measured. As depicted in Fig. 2b and c, the XPS spectra of the In and Sn elements in samples with two different deposited materials show a shifted binding energy. This indicates that both C3-D and C3-S can interact with the metal elements on the surface of ITO. It has been reported that N-containing conjugated heteroatomic groups serve as strong anchoring groups in organic light absorbers utilized in dye sensitized solar cells[47] and organic solar cells[48] for interacting with ITO. To gain a deeper understanding of the interactions between HTMs and ITO, we examined the XPS spectra of elements O, N, and S present in C3-D and C3-D. Since XPS measures the surface of the samples, we fabricated films of varying thickness to identify the key atoms that contribute more to the interaction with ITO. As depicted in Fig. 2d–f, the binding energy of O 1s and S 2p exhibits a noticeable shift, while the binding energy of N 1s shows very little shift. This suggests that the N atom is not involved in the interaction with ITO. Therefore, both C3-D and C3-S with added rhodanine group(s) may interact with ITO through C═O, C═S, or S atoms in the TT unit. This interaction is beneficial to the optimization of work function of ITO and the charge transfer from the HTM to the electrode. It is important to note that despite C3-S having two rhodanine groups with more heteroatoms, the interactions with ITO of C3-D and C3-S shown in XPS spectra are almost identical, as they exhibit the same shifted binding energy.

Table 1 Optical and electrochemical properties of C3-D and C3-S

HTM	E_{cutoff}[a] [eV]	E_{onset}[a] [eV]	λ_{onset} [nm]	E_g^{opt}[b] [eV]	E_{HOMO}[c] [eV]	E_{LUMO}[d] [eV]	$\mu_{h,sclc}$[e] [$cm^2 v^{-1} s^{-1}$]
C3-D	6.27	−9.66	626	1.98	−5.29	−3.31	1.29×10^{-4}
C3-S	6.36	−9.61	708	1.75	−5.25	−3.50	8.61×10^{-5}

[a] Determined by ultraviolet photoelectron spectroscopy (UPS) measurements. [b] Calculated according to the equation: $E_g^{opt} = 1240/\lambda_{onset}$ (eV). [c] Calculated according to the equation: $E_{HOMO} = -(21.22 - E_{cutoff} + E_{onset})$ (eV). [d] Calculated according to the equation: $E_{LUMO} = E_{HOMO} + E_g^{opt}$ (eV). [e] Measured by using the SCLC method.

2.3. The impact of HTMs on the perovskite layer

As the bottom layer, HTMs have various effects on the perovskite layer, such as nucleation, crystallization, morphology optimization and defect passivation.[14,16] Firstly, the water contact angle measurement was conducted to assess the hydrophobic surface of the HTM in inverted PSCs, which can promote the growth of high-quality perovskite polycrystalline films and provide some resistance to water permeation.[49] The test results showed that the water contact angle of C3-D is 100.37°, which is higher than that of C3-S (88.97°), indicating good hydrophobicity for both (Fig. S17, ESI†). Secondly, to investigate the impact of our hetero-atomic functional strategy on the interactions between the HTM and the perovskite layer, we conducted XPS measurements. As depicted in Fig. 3a and b, the binding energy of Pb 4f and I 3d at the interface between HTMs and perovskite shows a negative energy shift, suggesting the strong interactions between C3-D or C3-S and the perovskite layer, attributed to the coordination effects of the N, S, or O atoms in C3-D and C3-S.[50,51] Furthermore, we dissolved 0.5 mg of C3-D and 0.5 mg of C3-S in 1.0 mL of perovskite precursor solution, respectively, and performed the XPS tests of the corresponding films on ITO. As shown in Fig. 3c–e, in both C3-D and C3-S films, the signals

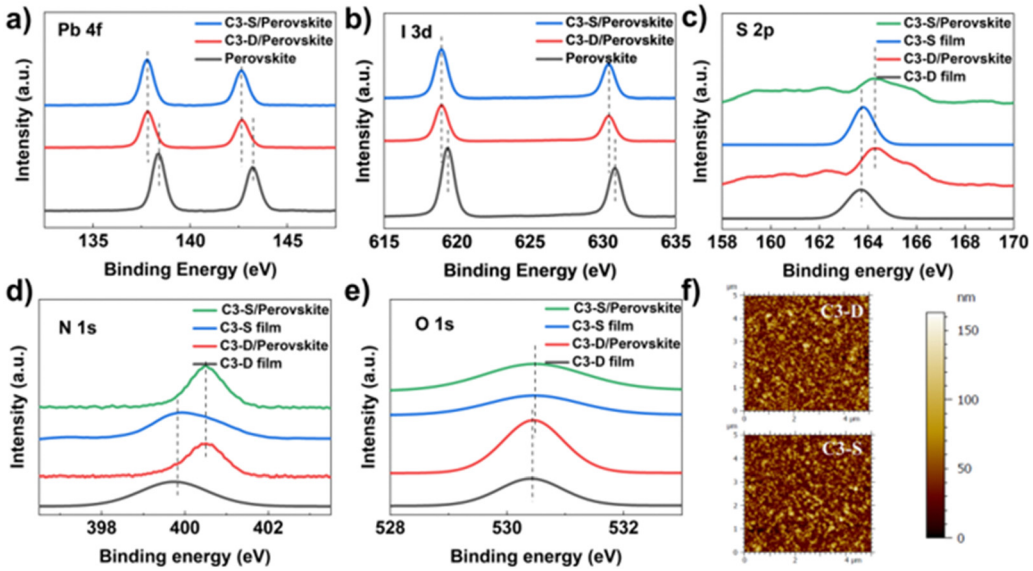

Fig. 3 XPS spectra of (a) Pb 3d, (b) I 3d, (c) S 2p, (d) N 1s and (e) O 1s for C3-D and C3-S deposited on ITO with different thickness; and (f) AFM images of C3-D and C3-S films.

of S 2p and N 1s demonstrate an evident energy shift, while the signal of O 1s atoms shows very little shift, indicating that the HTMs C3-D and C3-S may interact with the perovskite layer through C = S, or S and N atoms. Combining the XPS results of HTMs and ITO, it is understood that our new functionalized HTM with rhodanine efficiently improves the interfacial contact between ITO/HTM and HTM/perovskite layers, facilitating hole extraction and transport of cells. This shows promise for the enhancement of the performance of PSCs.

To investigate the impact of C3-D and C3-S on the crystallization of the perovskite layer, X-ray diffraction (XRD) experiments were carried out. As depicted in Fig. 4e, both the perovskite films on C3-D and C3-S exhibit the same peak positions. However, compared to the peak at 31.85° (−312), the intensities of the peaks at 14.22° (−111) and 28.44° (−222) are stronger in the film based on C3-D. Additionally, the half-peak width of the highest peaks at 14.22° (−111) is 0.23° (C3-D) and 0.26° (C3-S), respectively. The smaller half-peak width indicates the better crystallinity of perovskite films deposited on C3-D. Neither of the films show a noticeable peak at 12.70°, which is associated with (001) of the PbI_2 cubic phase in perovskite, suggesting that the perovskite layer is very pure. The scanning electron microscopy (SEM) measurements in top-view and cross-section were conducted to investigate the impact

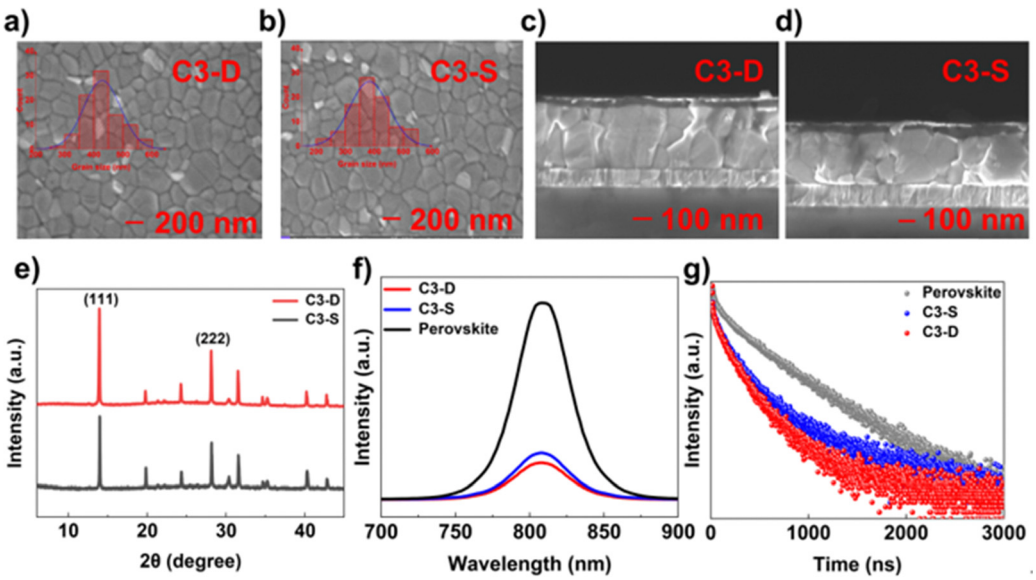

Fig. 4 SEM of perovskite film deposited on (a) C3-D, and (b) C3-S. Cross-sectional SEM of PSCs fabricated on (c) C3-D, and (d) C3-S. (e) XRD patterns of perovskite films deposited on C3-D and C3-S. (f) PL spectra and (g) TRPL spectra of perovskite films.

of C3-D and C3-S on the morphologies of the perovskite layer. As shown in Fig. 4a and b, the perovskite film on C3-D exhibits larger grain sizes with an average size of 428.87 nm and fewer grain boundaries compared to that on C3-S, which has an average grain size of 382.84 nm, based on the SEM analysis of the surface views of the perovskite layers. Additionally, in the cross-sectional view (Fig. 4c and d), the perovskite film based on C3-D also demonstrates higher crystal quality with a vertical orientation of crystal growth compared to the film based on C3-S. The high quality of the perovskite layers with larger grain sizes and fewer grain boundaries (GBs) may lead to a reduction in defects, ion migration, and nonradiative recombination in inverted PSCs.[52]

2.4. Photovoltaic performance

To investigate the impact of new functionalized HTMs, C3-D and C3-S, on the photovoltaic performance of PSCs, inverted planar PSCs were created using the ITO/C3-D or C3-S/perovskite/$PC_{61}BM$/BCP/Ag architecture (Fig. 5a). The light absorption layer used was the mixed-cation perovskite of $Cs_{0.05}FA_{0.95}PbI_3$. The energy levels of individual layers in the device structure are illustrated in Fig. 5b, with the energy levels and optical bandgaps of the perovskite and other layers being referenced from previous reports. In Fig. 5a, it is evident that while the HOMO energy levels of C3-D and C3-S closely align with the valence band maximum (VBM) of the perovskite (−5.38 eV), the HOMO energy level of C3-D (−5.29 eV) exhibits a better match with the perovskite layer compared to that of C3-S (−5.25 eV). This alignment is beneficial for hole extraction and reducing interfacial energy loss, indicating the superior performance of PSCs. After optimization, the devices achieved the highest PCEs at a HTM concentration of 4 mg mL^{-1}, and all the data are summarized in Table 2. Fig. 5c illustrates the *J–V* relationships of the champion PSC devices based on C3-D and C3-S under standard AM 1.5G illumination. The highest PCE of the best C3-D device reaches 21.50% with a V_{OC} = 1.072 V, J_{SC} = 24.49 mA cm^{-2} and FF = 81.9% in a reverse scan, while that of the best C3-S device is 19.24% with a V_{OC} = 1.065 V, J_{SC} = 23.11 mA cm^{-2} and FF = 78.2% in a reverse scan. The hysteresis of both devices during the forward–reverse scan is negligible. The results of external quantum efficiency (EQE) measurement (Fig. 5d) for C3-D devices demonstrate similar but stronger absorption ranges from 300 to 850 nm compared to C3-S. The maximum EQE value for C3-D-based devices is around 90%, while for C3-S-based devices it is around 85%. The integrated current density estimated from the EQE spectra is 23.96 mA cm^{-2} for C3-D and 22.18 mA cm^{-2} for C3-S, matching well with the J_{SC} values obtained from the *J–V* curves. Additionally, Fig. 5f shows the statistical distribution of PCE values for C3-D and C3-S devices. The devices based on C3-D exhibit a more centralized distribution, indicating better reproducibility in devices. Additionally, we tested the steady-state power output of PSCs at the maximum power point, and the stabilized power outputs for 300 s at a fixed voltage near the maximum power point are measured. As shown in Fig. 5e, the PCEs obtained from the stabilized power outputs are in good agreement with *J–V* output values, while the performance of C3-D-based devices is still better than the performance of devices based on C3-S.[53]

The *J–V* curves and EQE spectra indicate that C3-D-based devices exhibit a significant increase in V_{OC}, J_{SC}, and FF, and achieve more effective photogenerated carrier separation and conversion efficiency compared to C3-S, leading to improved PCEs. The enhanced V_{OC} could be due to the suppression of all-round defects, which in turn reduces nonradiative recombination (as discussed below) as well as the energy loss from the better energy level alignment, while the enhanced J_{SC} could be

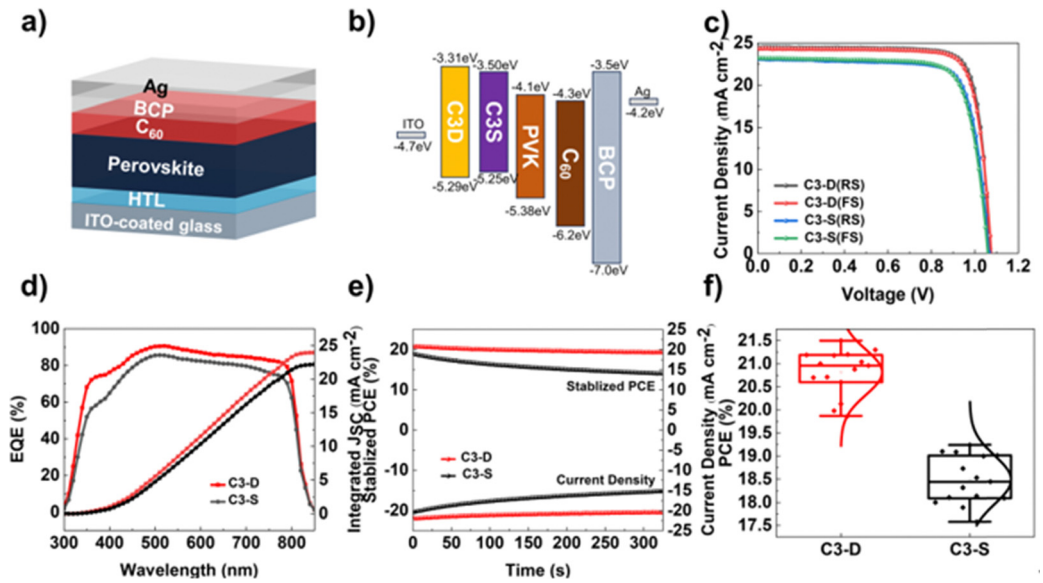

Fig. 5 (a) Device structure diagram; (b) diagram of the energy levels; (c) *J–V* curves measured by forward and reverse scans of the champion devices; (d) EQE spectrum and integrated short-circuit current density; (e) stability output curves at the maximum power point of the devices; and (f) the PCE statistics of devices.

Table 2 Performance of photovoltaic devices based on C3-D and C3-S

HTM	Scan direction	V_{OC} (V)	J_{SC} (mA cm^{-2})	FF (%)	PCE (%)
C3-D	Reverse	1.072	24.49	81.9	21.50
	Forward	1.076	24.33	81.0	21.20
C3-S	Reverse	1.065	23.11	78.2	19.24
	Forward	1.060	23.21	77.6	19.09

attributed to the high quality of the perovskite film including higher crystallinity, fewer GBs, *etc.* (as discussed above).

To investigate the carrier dynamics of the perovskite film influenced by HTMs, transient photocurrent (TPC) and transient photo-voltage (TPV) measurements[54] were conducted. As shown in Fig. S13 (ESI†), the carrier lifetime in TPC measurement slightly decreases from 14.87 μs (the device based on C3-S) to 14.75 μs (the device based on C3-D), indicating a little faster carrier extraction and transport in the C3-D device. Meanwhile, the longer lifetime of TPV indicates the longer lifetime of generated carriers in the open circuit state, demonstrating less non-radiative recombination in the device. TPV measurement (Fig. S16, ESI†) reveals that the carrier lifetime significantly increases from 469.08 μs for the C3-S device to 612.79 μs for the C3-D device, indicating reduced non-radiative recombination in the C3-D device, consistent with its higher V_{OC}. To further clarify the charge recombination kinetics in our PSCs, we performed a leakage current test based on the dark *J–V* curve of the devices. Fig. S18 (ESI†) illustrates that the device with C3-D exhibits lower leakage current in both negative and positive voltage regimes compared to the device with C3-S, indicating lower recombination in the device. We also measured the defect density of perovskite films using the space-charge limited current (SCLC) method, with a device structure of ITO/HTM/perovskite/MoO_3(10 nm)/Ag(100 nm). The concentration of the trap states in trap-filled region can be calculated based on eqn (1) as shown in Fig. S19 (ESI†):

$$V_{TFL} = \frac{qN_tL^2}{2\varepsilon_0\varepsilon_r} \quad (1)$$

where ε_r and ε_0 are the dielectric constants of perovskite and the vacuum permittivity, respectively, L is the thickness of the perovskite film, V_{TFL} is the trap-filled limited voltage, N_t is trap state concentrations and q is the elementary charge.[55] The concentrations of the trap states are correlated with V_{TFL}. The SCLC measurement reveals that the V_{TFL} decreases from 0.738 V to 0.494 V and the corresponding trap intensity N_t decreases from 6.80 × 1015 cm^{-3} (device based on C3-S) to 4.55 × 1015 cm^{-3} (device based on C3-D), indicating that C3-D contributes to better defect passivation at the interface of the perovskite layer compared to that of C3-S, thus reducing the energy loss to enhance the V_{OC}.[56–58] All these results are consistent with those of the TPV, TPC, and dark *J–V* curves.

To investigate the hole extraction of HTMs from perovskite, we conducted the steady-state photoluminescence (PL) tests. As depicted in Fig. 4f, all the steady-state PL emission peaks have a consistent wavelength of 810 nm. Compared to the bare perovskite, the PL intensities of the peak based on C3-D and C3-S were significantly reduced by 82% and 76%, respectively. The reduction is attributed to the extraction of holes from perovskite to the corresponding HTM. The weak PL peak based on C3-D indicates that there is a more efficient hole extraction process at the perovskite interface. The efficient interface charge transfer separation will contribute to a higher J_{SC}, which is consistent with the *J–V* tests.

The TRPL decay curves of perovskites on C3-D and C3-S are recorded to investigate the charge dynamics of the perovskite/HTM samples, and they can be fitted using the bi-exponential lifetime model according to the following equation:

$$I(t) = A_1 \exp\left(-\frac{\tau}{\tau_1}\right) + A_2 \exp\left(-\frac{\tau}{\tau_2}\right) + A_0 \quad (2)$$

in which A_1 and A_2 are fractions of two decay components, and τ_1 and τ_2 are the lifetimes responsible for the fast and slow recombination, respectively. The fitted τ_1 and τ_2 are listed in Table S2 (ESI†). Such a decay may be beneficial to the fast charge extraction or nanosecond time scaled nonradiative recombination losses in perovskite films. The fast decay (τ_1) is primarily related to the charge extraction speed and monomolecular defect-driven recombination, while the slow decay (τ_2) may be relevant to the non-radiative charge recombination.[59] As depicted in Fig. 4g and Table S2 (ESI†), in the perovskite/C3-D sample, the average lifetime (τ_{avg}) is 93.72 ns, with τ_1 = 4.56 ns and τ_2 = 179.58 ns. This is shorter than the τ_{avg} of 142.60 ns, τ_1 = 5.53 ns and τ_2 = 217.25 ns in the perovskite/C3-S sample. The shorter τ_1 in the perovskite/C3-D sample suggests that the interfacial charge transfer from the perovskite to C3-D is more efficient than that from the perovskite to C3-S. Additionally, C3-D is able to passivate trap states on the perovskite better than C3-S.

The stability of PSCs is a key parameter for assessing their potential for commercialization.[60] We first tested the stability of the champion devices based on C3-D and C3-S without any encapsulation. Both devices demonstrated very good stability, with a PCE retention of above 90% of their initial value after being stored for 500 hours in a 25 °C N_2 glovebox (Fig. 6a). Furthermore, when the unsealed device was heated at 85 °C for 500 hours in dark in a N_2 glovebox (Fig. 6b), the PCE of C3-D-based device remained above 60% of its initial value, demonstrating better thermal stability than that of C3-S-based device. Additionally, when kept in ambient air at 35% relative humidity at room temperature (Fig. 6c), the efficiency of the C3-D-based device remained above 85% of its initial value after aging for 500 hours, compared to the C3-S-based device the efficiency of which dropped to 80% of its initial efficiency at 200 hours. The improved ambient humidity and thermal stability of the C3-D-based device could be attributed to its relatively higher hydrophobicity and stronger interaction with ITO and the perovskite layer, which induced the growth of homogeneous perovskite crystallites with fewer surface defects and prevented undesirable air and water permeation.

It is worth noting that C3-D, with fewer hetero-atomic groups compared to C3-S, shows better device performance. As mentioned earlier, this can be attributed to the consistent interactions with ITO and defect passivation of C3-D and C3-S, as indicated in XPS measurements. The addition of another

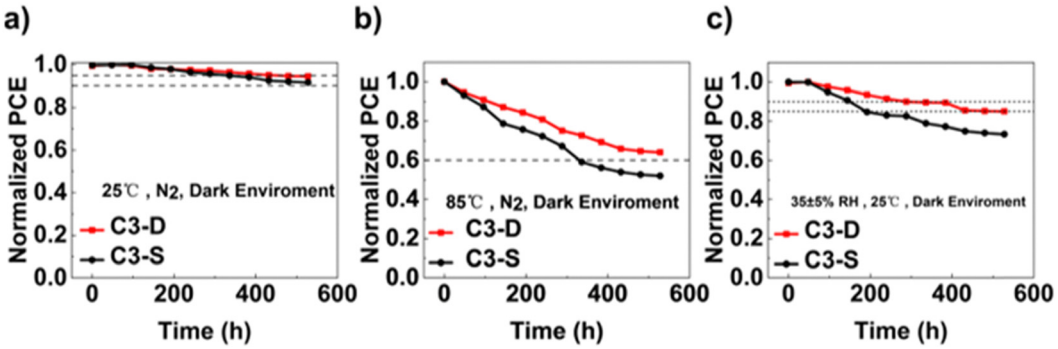

Fig. 6 (a) Nitrogen storage stability, (b) thermal stability and (c) ambient humidity stability of devices based on C3-D and C3-S.

rhodanine group may lead to poorer interfacial contact. The interfacial interaction between the HTL and perovskite is directly affected by the presence of polar groups in the two molecules. Moreover, the perovskite film deposited on C3-S exhibits smaller grains and more grain boundaries, potentially resulting in increased defects and suboptimal device performance. Furthermore, C3-D shows improved hole extraction and faster hole transfer from the perovskite layer to the electrode, along with reduced non-radiative recombination at the interface, leakage current, and defect density. However, in comparison to HTMs containing only thienothiophene–triphenylamine (TT-2,5-TPA),[43] the performance of PSCs based on C3-S also shows significant enhancement. Therefore, achieving superior device performance in the molecular design process requires a balance of hetero-atomic functional groups.

3. Conclusions

In summary, we synthesized two functionalized organic small molecule HTMs, C3-D and C3-S, with rhodanine units. With the functional group, both HTMs demonstrate good mobility, matching HOMO/LUMO energy levels and excellent interactions with ITO and the perovskite layer, enhancing hole extraction and transport and defect passivation in inverted PSCs. As a result, both devices of PSCs based on C3-D and C3-S display remarkable high PCE and stability compared to the non-functional HTM, TT-3,6-TPA, as reported in the literature,[43] and the champion device based on C3-D yields a high PCE of 21.50% with J_{SC} = 24.49 mA cm^{-2}, V_{OC} = 1.072 V, and FF = 81.9% under standard AM 1.5G illumination. After being kept for 500 hours at room temperature in ambient air in the dark at 35% relative humidity, the PCE is still retained at more than 85% of the initial value. In contrast, for the non-functional HTM, TT-3,6-TPA, the highest PCE is only 0.7% with J_{SC} = 2.90 mA cm^{-2}, V_{OC} = 0.95 V, and FF = 27.0% as reported in the literature. In conclusion, our functional strategy and results may open up a new avenue for designing highly efficient HTMs for high-performance inverted PSCs.

Data availability

The data supporting this article have been included as part of the ESI.†

Conflicts of interest

There are no conflicts to declare.

Acknowledgements

This work is supported by the National Key Research and Development Program of China (2022YFB4200305); the National Natural Science Foundation of China (22075140; 22279039; 22272115; and 22202145); the Chinese National 1000-Talent-Plan program; the Frontier Project of the Application Foundation of Wuhan Science and Technology Plan Project (2020010601012202); the Innovation Project of Optics Valley Laboratory (OVL2021BG008); and the Science and Technology Plan Project of Taizhou (23gya05). The authors thank the Analytical and Testing Centre from HUST and the Centre for Nanoscale Characterization and Devices (CNCD) from WNLO (HUST) for the facility support of sample measurements.

References

1 T.-H. Han, S. Tan, J. Xue, L. Meng, J.-W. Lee and Y. Yang, Interface and Defect Engineering for Metal Halide Perovskite Optoelectronic Devices, *Adv. Mater.*, 2019, **31**, 1803515.
2 Y. Rong, Y. Hu, A. Mei, H. Tan, M. I. Saidaminov, S. I. Seok, M. D. McGehee, E. H. Sargent and H. Han, Challenges for commercializing perovskite solar cells, *Science*, 2018, **361**, eaat8235.
3 S. I. Seok, M. Grätzel and N.-G. Park, Methodologies toward highly efficient perovskite solar cells, *Small*, 2018, **14**, 1704177.
4 F. H. Isikgor, S. Zhumagali, L. V. Merino, M. De Bastiani, I. McCulloch and S. De Wolf, Molecular engineering of contact interfaces for high-performance perovskite solar cells, *Nat. Rev. Mater.*, 2023, **8**, 89.
5 G. Nazir, S.-Y. Lee, J.-H. Lee, A. Rehman, J.-K. Lee, S. I. Seok and S.-J. Park, Stabilization of perovskite solar cells: recent developments and future perspectives, *Adv. Mater.*, 2022, **34**, 2204380.
6 A. Kojima, K. Teshima, Y. Shirai and T. Miyasaka, Organometal halide perovskites as visible-light sensitizers for photovoltaic cells, *J. Am. Chem. Soc.*, 2009, **131**, 6050.
7 NREL, Best Research-Cell Efficiencies, **https://www.nrel.gov/pv/cell-efficiency.html**, (accessed December 2023).

8 X. Lin, D. Cui, X. Luo, C. Zhang, Q. Han, Y. Wang and L. Han, Efficiency progress of inverted perovskite solar cells, *Energy Environ. Sci.*, 2020, **13**, 3823.
9 C. Gao, D. Du, D. Ding, F. Qiaoa and W. Shen, A review on monolithic perovskite/c-Si tandem solar cells: progress, challenges, and opportunities, *J. Mater. Chem. A*, 2022, **10**, 10811.
10 Y. Jiang, S. He, L. Qiu, Y. Zhao and Y. Qi, Perovskite solar cells by vapor deposition based and assisted methods, *Appl. Phys. Rev.*, 2022, **9**, 021305.
11 S. Aftab, S. Hussain, F. Kabir, M. Aslam, A. H. Rajpar and A. G. Al-Sehemi, Advances in flexible perovskite solar cells: A comprehensive review, *Nano Energy*, 2024, **120**, 109112.
12 K. Wang, L. Zheng, Y. Hou, A. Nozariasbmarz, B. Poudel, J. Yoon, T. Ye, D. Yang, A. V. Pogrebnyakov, V. Gopalan and S. Priya, Overcoming Shockley-Queisser limit using halide perovskite platform?, *Joule*, 2022, **6**, 756.
13 C.-H. Lin, L. Hu, X. Guan, J. Kim, C.-Y. Huang, J.-K. Huang, S. Singh and T. Wu, Electrode engineering in halide perovskite electronics: plenty of room at the interfaces, *Adv. Mater.*, 2022, **34**, 2108616.
14 R. Dai, X. Meng, J. Zhang, Z. Cai, L. Tan and Y. Chen, Preburied Interface Strategy for Stable Inverted Perovskite Solar Cells Based on Ordered Nucleation Crystallization, *Adv. Funct. Mater.*, 2023, **33**, 2305013.
15 Z. Pan, D. Peng, X. Zhao, W. Xu, Y. Bao, Z. Feng, Q. Zou, B. Xu, Y. Wang, H. Gao, C. Yin, R. Li, J. Wang and W. Huang, Side-Chain Functionalized Polymer Hole-Transporting Materials with Defect Passivation Effect for Highly Efficient Inverted Quasi-2D Perovskite Solar Cells, *Adv. Funct. Mater.*, 2023, **33**, 2304881.
16 M. Luo, X. Zong, M. Zhao, Z. Sun, Y. Chen, M. Liang, Y. Wu and S. Xue, *Chem. Eng. J.*, 2022, **442**, 136136.
17 B. Yang, D. Bogachuk, J. Suo, L. Wagner, H. Kim, J. Lim, A. Hinsch, G. Boschloo, M. K. Nazeeruddin and A. Hagfeldt, Strain effects on halide perovskite solar cells, *Chem. Soc. Rev.*, 2022, **51**, 7509.
18 S. Park, D. W. Kim and Y. Park, Improved stability and efficiency of inverted perovskite solar cell by employing nickel oxide hole transporting material containing ammonium salt stabilizer, *Adv. Funct. Mater.*, 2022, **32**, 2200437.
19 J. Y. Kim, J.-W. Lee, H. S. Jung, H. Shin and N.-G. Park, High-efficiency perovskite solar cells, *Chem. Rev.*, 2020, **120**, 7867.
20 Q. Cao, T. Wang, X. Pu, X. He, M. Xiao, H. Chen, L. Zhuang, Q. Wei, H.-L. Loi, P. Guo, B. Kang, G. Feng, J. Zhuang, G. Feng, X. Li and F. Yan, Co-Self-Assembled Monolayers Modified NiOx for Stable Inverted Perovskite Solar Cells, *Adv. Mater.*, 2024, **36**, 2311970.
21 B. Li, C. Zhang, D. Gao, X. Sun, S. Zhang, Z. Li, J. Gong, S. Li and Z. Zhu, Suppressing Oxidation at Perovskite–NiO_x Interface for Efficient and Stable Tin Perovskite Solar Cells, *Adv. Mater.*, 2023, **36**, 2309768.
22 S. Yu, Z. Xiong, H. Zhou, Q. Zhang, Z. Wang, F. Ma, Z. Qu, Y. Zhao, X. Chu, X. Zhang and J. You, Homogenized NiOx nanoparticles for improved hole transport in inverted perovskite solar cells, *Science*, 2023, **382**, 1399.
23 M. Jeong, I. W. Choi, E. M. Go, Y. Cho, M. Kim, B. Lee, S. Jeong, Y. Jo, H. W. Choi, J. Lee, J.-H. Bae, S. K. Kwak, D. S. Kim and C. Yang, Stable perovskite solar cells with efficiency exceeding 24.8% and 0.3 V voltage loss, *Science*, 2020, **369**, 1615.
24 X. Wu, D. Gao, X. Sun, S. Zhang, Q. Wang, B. Li, Z. Li, M. Qin, X. Jiang, C. Zhang, Z. Li, X. Lu, N. Li, S. Xiao, X. Zhong, S. Yang, Z. A. Li and Z. Zhu, Backbone Engineering Enables Highly Efficient Polymer Hole-Transporting Materials for Inverted Perovskite Solar Cells, *Adv. Mater.*, 2023, **35**, 2208431.
25 H. D. Pham, L. Xianqiang, W. Li, S. Manzhos, A. K. K. Kyaw and P. Sonar, Organic interfacial materials for perovskite-based optoelectronic devices, *Energy Environ. Sci.*, 2019, **12**, 1177.
26 H. Kim, D. Y. Lee, J. Lim, J. Kim, J. Park, J. Seidel, J. S. Yun and S. I. Seok, Enhancing Stability and Efficiency of Perovskite Solar Cells with a Bilayer Hole Transporting Layer of Nickel Phthalocyanine and Poly(3-Hexylthiophene), *Adv. Energy Mater.*, 2023, **13**, 2301046.
27 C. Zhang, K. Wei, J. Hu, X. Cai, G. Du, J. Deng, Z. Luo, X. Zhang, Y. Wang, L. Yang and J. Zhang, A review on organic hole transport materials for perovskite solar cells: Structure, composition and reliability, *Mater. Today*, 2023, **67**, 518.
28 C.-M. Hung, C.-C. Wu, P.-H. Tsao, C.-D. Lung, C.-H. Wang, I. C. Ni, C.-C. Chu, C.-H. Cheng, W.-Y. Kuang, C.-I. Wu, H.-C. Chen, Y.-T. Chan and P.-T. Chou, Functionalization of Donor–π–Acceptor Hole Transport Materials Enhances Crystallization and Defect Passivation in Inverted Perovskite Solar Cells: Achieving Power Conversion Efficiency >21% (Area: 1.96 cm2) and Impressive Stability, *Adv. Energy Sustainability Res.*, 2023, **4**, 2300042.
29 M. Liu, M. Li, Y. Li, Y. An, Z. Yao, B. Fan, F. Qi, K. Liu, H.-L. Yip, F. R. Lin and A. K. Y. Jen, Defect-Passivating and Stable Benzothiophene-Based Self-Assembled Monolayer for High-Performance Inverted Perovskite Solar Cells, *Adv. Energy Mater.*, 2024, **14**, 2303742.
30 E. Hytham, S. Hiroo, N. Takeshi, A. K. K. Kyaw and H. Yasuhiko, Phenolphthalein: A Potent Small-Molecule Additive for High-Performance and Ambient-Air-Stable FAPbI3 Perovskite Solar Cells, *ACS Appl. Energy Mater.*, 2023, **7**, 2925–2937.
31 X. Sun, H. Fan, M. Rauf, X. Xu, G. Li, X. Gu, D. Luo, C. Shan, Q. Yang, S. Dong, C. Miao, Z. Xie, G. Lu, D. Wang, P. Sun and A. K. K. Kyaw, A Fluorination Strategy and Low-Acidity Anchoring Group in Self-Assembled Molecules for Efficient and Stable Inverted Perovskite Solar Cells, *Chem. - Eur. J.*, 2024, **30**, e202400629.
32 M. Abbas, X. Xu, M. Ruaf and A. K. K. Kyaw, A Comprehensive Review on Defects-Induced Voltage Losses and Strategies toward Highly Efficient and Stable Perovskite Solar Cells, *Photonics*, 2024, **11**, 87.
33 M. Li, J. Chang, R. Sun, H. Wang, Q. Tian, S. Chen, J. Wang, Q. He, G. Zhao, W. Xu, Z. Li, S. Zhang, F. Wang and T. Qin, Underlying Interface Defect Passivation and Charge

Transfer Enhancement via Sulfonated Hole-Transporting Materials for Efficient Inverted Perovskite Solar Cells, *ACS Appl. Mater. Interfaces*, 2022, **14**, 53331.

34 R. Li, J. Zhang, M. Liu, S. K. Matta, J. Tian, Z. Deng, S. P. Russo, P. Vivo, Z. Zhou and H. Zhang, Synergistic Fluorine Sulfur Intra- and Intermolecular Interactions on Dopant-Free Hole Transport Material for Efficient and Stable Inverted Perovskite Solar Cells, *Solar RRL*, 2023, **7**, 2300031.

35 Y. Li, H. Fan, F. Xu, T. Wang, C. Shan, W. Li, X. Gu, X. Lai, D. Luo, Z. Sun, M. Zhao, X. Li, K. Cui, G. Li and A. K. K. Kyaw, High-Performance Inverted Perovskite Solar Cells Enhanced via Partial Replacement of Dimethyl Sulfoxide with N-Methyl-2-Pyrrolidinone, *Solar RRL*, 2022, **6**, 2200816.

36 Z.-R. Lan, J.-Y. Shao and Y.-W. Zhong, Self-assembled monolayers as hole-transporting materials for inverted perovskite solar cells, *Mol. Syst. Des. Eng.*, 2023, **8**, 1440.

37 X. Sun, Z. Zhu and Z. Li, Recent advances in developing high-performance organic hole transporting materials for inverted perovskite solar cells, *Front. Optoelectron.*, 2022, **15**, 46.

38 S. Wang, H. Guo and Y. Wu, Advantages and challenges of self-assembled monolayer as a hole-selective contact for perovskite solar cells, *Mater. Futures*, 2023, **2**, 012105.

39 Y. Yao, C. Cheng, C. Zhang, H. Hu, K. Wang and S. De Wolf, Organic Hole-Transport Layers for Efficient, Stable, and Scalable Inverted Perovskite Solar Cells, *Adv. Mater.*, 2022, **34**, 2203794.

40 N. Cai, F. Li, Y. Chen, R. Luo, T. Hu, F. Lin, S.-M. Yiu, D. Liu, D. Lei, Z. Zhu and A. K. Y. Jen, Synergistical Dipole–Dipole Interaction Induced Self-Assembly of Phenoxazine-Based Hole-Transporting Materials for Efficient and Stable Inverted Perovskite Solar Cells, *Angew. Chem., Int. Ed.*, 2021, **60**, 20437.

41 Q. Liao, Y. Wang, Z. Zhang, K. Yang, Y. Shi, K. Feng, B. Li, J. Huang, P. Gao and X. Guo, Self-assembled donor-acceptor hole contacts for inverted perovskite solar cells with an efficiency approaching 22%: The impact of anchoring groups, *J. Energy Chem.*, 2022, **68**, 87.

42 S. Zhang, R. Wu, C. Mu, Y. Wang, L. Han, Y. Wu and W.-H. Zhu, Conjugated Self-Assembled Monolayer as Stable Hole-Selective Contact for Inverted Perovskite Solar Cells, *ACS Mater. Lett.*, 2022, **4**, 1976.

43 T. H. Le, Q.-D. Dao, M.-P. Nghiêm, S. Péralta, R. Guillot, Q. N. Pham, A. Fujii, M. Ozaki, F. Goubard and T.-T. Bui, Triphenylamine–Thienothiophene Organic Charge-Transport Molecular Materials: Effect of Substitution Pattern on their Thermal, Photoelectrochemical, and Photovoltaic Properties, *Chem.–Asian J.*, 2018, **13**, 1302.

44 T. Soya and A. Osuka, Internally Bridged Hückel Aromatic [4,6]Decaphyrins: (Doubly-Twisted-Annuleno)Doubly-Twisted-Annulene Variants, *Chem. – Eur. J.*, 2019, **25**, 5173–5176.

45 Y. Zhang, G. Cai, Y. Li, Z. Zhang, T. Li, X. Zuo, X. Lu and Y. Lin, An Electron Acceptor Analogue for Lowering Trap Density in Organic Solar Cells, *Adv. Mater.*, 2021, **33**, 2008134.

46 Y. Hua, S. Chen, D. Zhang, P. Xu, A. Sun, Y. Ou, T. Wu, H. Sun, B. Cui and X. Zhu, Bis[di(4-methoxyphenyl)amino]carbazole-capped indacenodithiophenes as hole transport materials for highly efficient perovskite solar cells: the pronounced positioning effect of a donor group on the cell performance, *J. Mater. Chem. A*, 2019, **7**, 10200.

47 J. Cui, J. Lu, X. Xu, K. Cao, Z. Wang, G. Alemu, H. Yuang, Y. Shen, J. Xu, Y. Cheng and M. Wang, Organic Sensitizers with Pyridine Ring Anchoring Group for p-Type Dye-Sensitized Solar Cells, *J. Phys. Chem. C*, 2014, **118**, 16433.

48 G. Chen, S. Liu, Z. He, H.-B. Wu, W. Yang, B. Zhang and Y. Cao, Pyridine-incorporated alcohol-soluble neutral polyfluorene derivatives as efficient cathode-modifying layers for polymer solar cells, *Polym. Chem.*, 2017, **8**, 6720.

49 C. Bi, Q. Wang, Y. Shao, Y. Yuan, Z. Xiao and J. Huang, Non-wetting surface-driven high-aspect-ratio crystalline grain growth for efficient hybrid perovskite solar cells, *Nat. Commun.*, 2015, **6**, 7747.

50 R. Chen, S. Liu, X. Xu, F. Ren, J. Zhou, X. Tian, Z. Yang, X. Guanz, Z. Liu, S. Zhang, Y. Zhang, Y. Wu, L. Han, Y. Qi and W. Chen, Robust hole transport material with interface anchors enhances the efficiency and stability of inverted formamidinium–cesium perovskite solar cells with a certified efficiency of 22.3%, *Energy Environ. Sci.*, 2022, **15**, 2567.

51 X. Yang, D. Luo, Y. Xiang, L. Zhao, M. Anaya, Y. Shen, J. Wu, W. Yang, Y.-H. Chiang, Y. Tu, R. Su, Q. Hu, H. Yu, G. Shao, W. Huang, T. P. Russell, Q. Gong, S. D. Stranks, W. Zhang and R. Zhu, Buried Interfaces in Halide Perovskite Photovoltaics, *Adv. Mater.*, 2021, **33**, 2006435.

52 J. Jiang, Q. Wang, Z. Jin, X. Zhang, J. Lei, H. Bin, Z.-G. Zhang, Y. Li and S. F. Liu, Polymer Doping for High-Efficiency Perovskite Solar Cells with Improved Moisture Stability, *Adv. Energy Mater.*, 2018, **8**, 1701757.

53 F. Meng, Y. Wang, Y. Wen, X. Lai, W. Li, A. K. K. Kyaw, R. Zhang, D. Fan, Y. Li, M. Du, X. Guo, H. Ma, G. Li, X. W. Sun and J. Wang, Dopant-Free and Green-Solvent-Processable Hole-Transporting Materials for Highly Efficient Inverted Planar Perovskite Solar Cells, *Solar RRL*, 2020, **4**, 2000327.

54 T. M. Clarke, C. Lungenschmied, J. Peet, N. Drolet and A. J. Mozer, A Comparison of Five Experimental Techniques to Measure Charge Carrier Lifetime in Polymer/Fullerene Solar Cells, *Adv. Energy Mater.*, 2015, **5**, 1401345.

55 Z. Yao, W. Zhao, Z. Xu, J. Wen and S. F. Liu, Morphology Evolution of a High-Efficiency PSC by Modulating the Vapor Process, *Small*, 2020, **16**, 2003582.

56 Y. Yang, W. Zhao, T. Yang, J. Liu, J. Zhang, Y. Fang and S. Liu, Design of surface termination for high-performance perovskite solar cells, *J. Mater. Chem. A*, 2021, **9**, 23597–23606.

57 S. Jeong, S. Seo, H. Yang, H. Park, S. Shin, H. Ahn, D. Lee, J. H. Park, N. G. Park and H. Shin, Cyclohexylammonium-Based 2D/3D Perovskite Heterojunction with Funnel-Like Energy Band Alignment for Efficient Solar Cells (23.91%), *Adv. Energy Mater.*, 2021, **11**, 2102236.

58 Y. Li, D. Fan, F. Xu, C. Shan, J. Yu, W. Li, D. Luo, Z. Sun, H. Fan, M. Zhao, X. Li, K. Cui, R. Chen, G. Li and

A. K. K. Kyaw, 1 + 1 > 2: Dual strategies of quinolinic acid passivation and DMF solvent annealing for high-performance inverted perovskite solar cell, *Chem. Eng. J.*, 2022, **435**, 135107.
59 W. Tress, Perovskite Solar Cells on the Way to Their Radiative Efficiency Limit – Insights Into a Success Story of High Open-Circuit Voltage and Low Recombination, *Adv. Energy Mater.*, 2017, **7**, 1602358.
60 C. Xu, Z. Liu and E.-C. Lee, Stability and efficiency improved perovskite solar cells through tuning the hydrophobicity of the hole transport layer with an organic semiconductor, *J. Mater. Chem. C*, 2021, **9**, 679.

